

Electron scale nested quadrupole Hall field in Cluster observations of magnetic reconnection

Neeraj Jain

*Max Planck Institute for Solar System Research,
Justus-von-Liebig-Weg-3, Göttingen, Germany.*

A. Surjalal Sharma

Department of Astronomy, University of Maryland, College Park, MD 20742, USA.

(Dated: September 14, 2021)

Abstract

This Letter presents the first evidence of a new and unique feature of spontaneous reconnection at multiple sites in electron current sheet, viz. nested quadrupole structure of Hall field at electron scales, in Cluster observations. The new nested quadrupole is a consequence of electron scale processes in reconnection. Whistler response of the upstream plasma to the interaction of electron flows from neighboring reconnection sites produces a large scale quadrupole Hall field enclosing the quadrupole fields of the multiple sites, thus forming a nested structure. Electron-magnetohydrodynamic simulations of an electron current sheet yields mechanism of the formation of nested quadrupole.

Magnetic reconnection is a fundamental process for the fast release of magnetic energy into kinetic and thermal energy in laboratory, space and astrophysical plasmas. Collisionless reconnection develops in thin current sheets with thicknesses comparable to the electron skin depth $d_e (= c/\omega_{pe})$. The electron current sheet (ECS) with thickness $\sim d_e$ is embedded inside an ion current sheet with thickness $\sim d_i (= c/\omega_{pi})$. The electron and ion dynamics are decoupled at this scale and the plasma is no longer frozen in the magnetic field, thus enabling reconnection. The Hall current due to the differential flow of ions and electrons in the reconnection region generates an out-of-plane magnetic field with a quadrupolar structure [1, 2], which will be referred to as the Hall field. The quadrupole structure of the Hall field is an essential feature of collisionless reconnection and has been detected in space observations [3–5], laboratory experiments [6] and simulations [7].

The electron current sheet is susceptible to secondary tearing instabilities which lead to spontaneous reconnection at multiple sites in ECS [8]. The interaction of neighboring sites leads to a new and unique feature, viz. nested quadrupole structure of the Hall field [9], unlike the single quadrupole in the case of reconnection at a single site. This feature arises in electron current sheets with a thickness (\sim few d_e) which is small compared to its extent (\sim few d_i). Such current sheets are unstable to tearing instability, with a growth rate that has a maximum when the perturbation has scale length of a few d_e [9, 10], thus leading to reconnection at multiple sites. This Letter presents the first evidence of a nested quadrupole structure of Hall field in the Cluster observations of an electron scale current sheet in Earth’s magnetotail [3]. The Cluster spacecraft crossed the reconnection region at distances of $\sim 18R_E$ in Earth’s magnetotail on 1 October 2001. Among the four spacecraft SC4 was closest to the X-line and crossed the current sheet on the earthward side between 09:46:48 and 09:46:51 UT, and the profiles of electric and magnetic field are shown in Fig. 1 (Fig. 3 in Ref. [3]). The change in sign of the magnetic field components are critical to the structure of the Hall field and the time marks for these are shown by the vertical dashed lines in Fig. 1, viz. L_1 for B_z , L_2 for B_y , L_3 for B_z , and L_4 for B_x and B_y .

A schematic of the magnetic field structure corresponding to the Cluster observations (Fig. 1) is shown in Fig. 2, and consists of a primary site, with X-point at P, and a secondary site with X-point at S. In the standard picture of 2-D reconnection with a single reconnection site, i. e., in the absence of the secondary sites, B_z should have the same sign on any one side (tail-ward or earthward) of the $y - z$ plane containing the X-point P, and

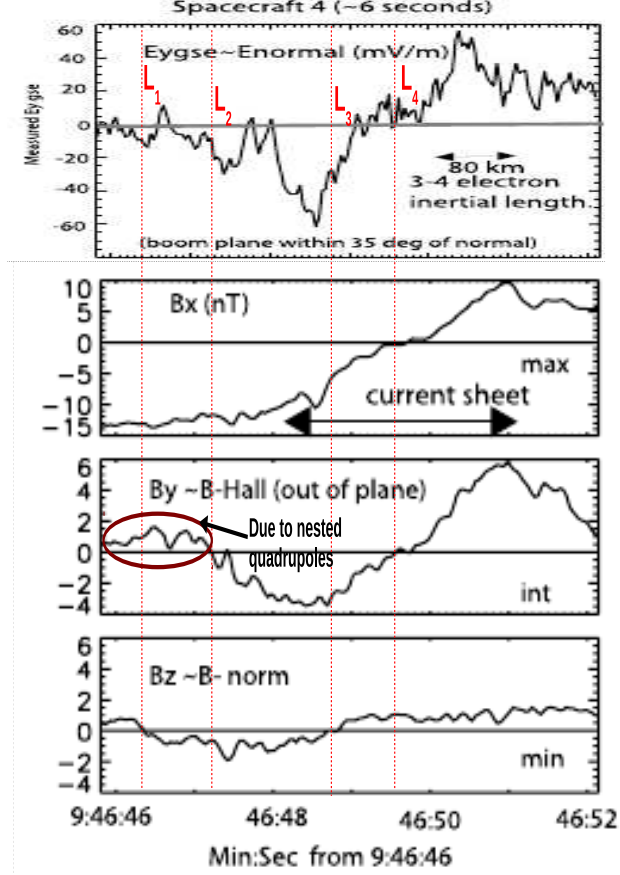


FIG. 1. Observation of electron scale current sheet by Cluster (adopted from Fig. 3a of [3]). (top panel) E_{yGSE} (y -component of electric field in GSE coordinate system). (Three bottom panels) x , y and z components of magnetic field in boundary normal coordinate system. Vertical dashed lines ($L_1 - L_4$) mark the zero crossings of the magnetic field components.

change sign only when spacecraft crosses this plane. But for such a passage by a spacecraft, the peak of the out-of-plane Hall field (B_y) should not coincide with the zero crossing of the normal magnetic field (B_z). This is because the peaks of the Hall field are located away from this plane, as seen in the Cluster data (Line L_3). Thus the change of sign of B_z at L_3 coinciding with the peak of the Hall field is not consistent with reconnection at a single site. The change of sign of B_z without crossing an X-point is possible, however, when spacecraft crosses the current sheet between a primary (P) and a secondary (S) reconnection sites, e.g., along the dashed line in Fig. 2. The spacecraft first encounters magnetic field lines (at A with positive B_z) reconnected at the primary site P but not reconnected at the secondary site S. It then encounters the field lines of the magnetic island formed due to the

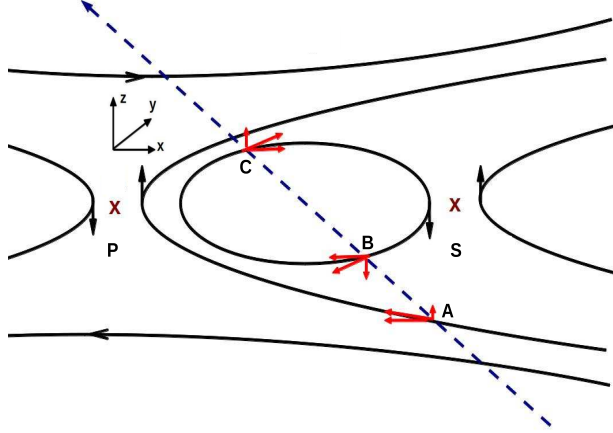


FIG. 2. A schematic of reconnection at a primary (P) and a secondary (S) sites. Components of the magnetic field in x and z directions are shown by red arrows at select locations (A, B and C) on a spacecraft trajectory (blue dashed line).

reconnection both at P and S, first in the region below the plane containing the primary and secondary sites, viz. the south lobe (at B with negative B_z) and then in the north lobe (at C with positive B_z). Although the presence of a magnetic island between the two reconnection sites P and S is enough for the sign reversal of B_z at L_3 and B_y at L_4 , the small positive B_z on the left of L_1 and B_y on the left of L_2 additionally require the weak or secondary site to be inside the region created by the dominant or primary site.

The correspondence of the Cluster observations of the magnetic field (Fig. 1) to reconnection at multiple sites is modeled using electron-magnetohydrodynamic (EMHD) simulations of spontaneous reconnection in an ECS developing into primary and secondary sites [9], shown in Fig. 3. Here length is normalized by d_e , magnetic field by the asymptotic value B_0 and time by $\omega_{ce}^{-1} = (eB_0/m_e)^{-1}$. The profiles of electric and magnetic fields in the simulations along a possible spacecraft trajectory (shown by the thick line with an arrow in Fig. 3b) are shown in Fig. 4. Fig. 3a shows the structure of the Hall field B_y in the early stage ($\omega_{cet} = 45$), which evolves into the late stage ($\omega_{cet} = 145$), shown in Fig. 3b. At $\omega_{cet} = 45$ the reconnection is dominant at the primary site (P) in the center of the simulation domain ($x = z = 0$). The field lines reconnected at the primary site P reconnect again at the secondary sites, (S_1 at $x \approx -16d_e$ and S_2 at $x \approx 16d_e$), giving rise to reconnection at multiple

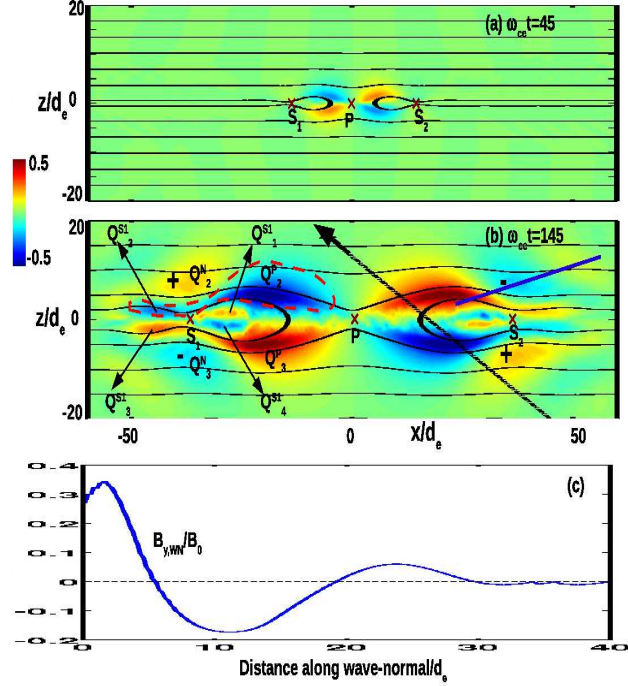


FIG. 3. Magnetic field lines (black) plotted over color coded B_y at $\omega_{ce}t = 45$ (a) and $=145$ (b). The primary (P) and secondary (S_1 and S_2) sites are marked by cross (\times). At $\omega_{ce}t = 145$, outward oblique propagation of whistlers from secondary sites forms a new quadrupole, marked with '+' and '-'. In (b), the poles of primary, secondary and new quadrupoles are marked by Q's (see text for definition) in the left half. The red-dashed loop encloses a negative pole of the extended quadrupole. The blue line in the top-right quadrant is at an angle of 19.5 degrees with the background magnetic field along $+x$ and approximates the wave normal. The profile of B_y along the wave normal is shown in (c). The black line with an arrow in (b) shows a possible trajectory of Cluster spacecraft.

sites. The quadrupole structure of the out-of-plane magnetic field is clearly developed around the primary site, while it is not recognizable yet at the secondary sites. At $\omega_{ce}t = 145$, the central site remains dominant and the secondary sites are pushed away by the outflows from the central site. We label the quadrupole Hall fields associated with S_1 , S_2 and P by Q^{S_1} , Q^{S_2} and Q^P , respectively. The new quadrupole, marked as Q^N , forms due to the interactions of the inflow to the secondary sites and the outflow from the primary site [9]. The poles of a quadrupole are numbered counter clockwise beginning with 1 for the top right pole to 4 for the bottom right pole. An individual pole of a quadrupole is represented by a subscript to

Q's. For example, $Q_1^{S_1}$ represents the top right pole of the quadrupole associated with the reconnection site S_1 . The poles of the primary, secondary and new quadrupoles are marked only in the left half of Fig. 3b. The poles $Q_1^{S_1}$ and $Q_4^{S_1}$ of the secondary quadrupole at S_1 penetrates between the poles Q_2^P and Q_3^P of primary quadrupole. At the same time, the poles $Q_2^{S_1}$ and $Q_3^{S_1}$ of the secondary quadrupole at S_1 connect to the poles Q_2^P and Q_3^P of the primary quadrupole, respectively, thus increasing the extent of the primary quadrupole Q^P . One of the negative pole ($Q_2^P + Q_2^{S_1}$) of the extended quadrupole is enclosed by a closed loop (red dashed line) in Fig. 3b. The extended quadrupole is nested inside the new quadrupole (Q^N), the poles of which are also marked ('+' and '-') in Fig. 3b.

A striking feature of spontaneous reconnection at multiple sites is the new quadrupole which, unlike the other three quadrupoles in Fig. 3b, is not directly associated with a reconnection site but arises from their interaction. The physics of the new quadrupole is the whistler response of the upstream plasma to the interaction of inflow to the secondary (weak) sites and outflow from the primary (dominant) site [9]. Because of the magnetic field structure of reconnection, the whistler perturbations are anchored in phase at their origin and propagate away from the reconnection region. The direction of propagation is very well approximated by the wave normal (shown by blue line in Fig. 3b) which is at Storey angle of 19.5° [11, 12] with the background magnetic field along x . Fig. 3c shows the out-of-plane magnetic field $B_{y,WN}$ along the wave normal. The wave propagates away from the reconnection region while its amplitude diminishes. The distance between positive and negative peaks is $\approx 12d_e$ giving a wavenumber $kd_e \approx 0.25$, as expected for frequency $\omega = 0.1\omega_{ce}$ [13]. The extension of the primary quadrupole along x , and, the formation of a new quadrupole due to the whistler perturbation at secondary sites in the manner described above make the overall structure a nested structure of quadrupoles.

Fig. 4 shows the profiles of electric and magnetic fields (in un-normalized units using $B_0 = 10$ nT and $d_e = 20$ km for Cluster observations) along the trajectory shown in Fig. 3b, as functions of distance along the trajectory. Similar to Fig. 1, the vertical dashed lines in this figure mark the zero crossing of B_x at L_4 , B_y at L_2 and L_4 , and B_z at L_1 and L_3 . The profiles of the y -component of electric field and all components of magnetic field in Fig. 1 are in the Geocentric Solar Ecliptic (GSE) and boundary normal coordinate systems, respectively. In the boundary normal coordinate system, z is normal to the current sheet surface, y is along the direction of current and (x, y, z) forms a right handed coordinate

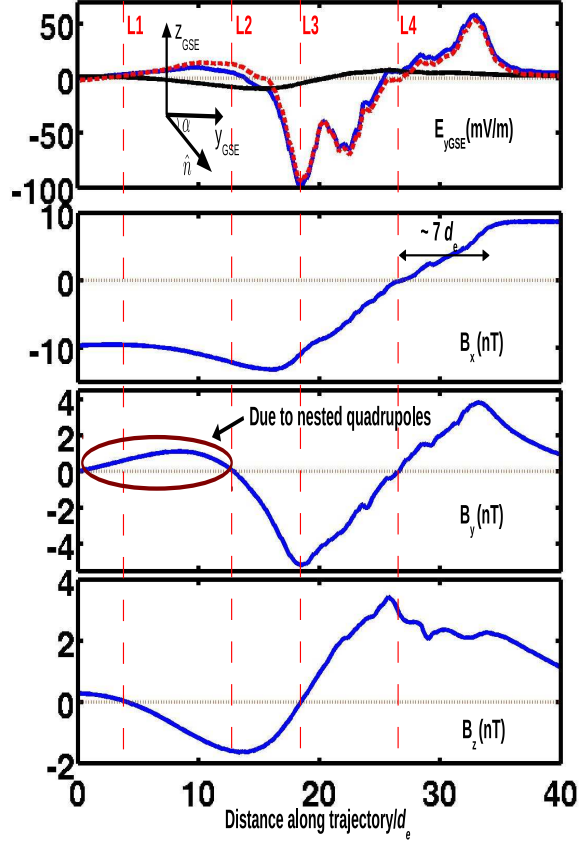


FIG. 4. Simulated electric and magnetic field profiles along the trajectory shown in Fig. 3b. (top panel) The y -component of electric field (E_{yGSE} , blue) transformed from the simulation or boundary normal to GSE coordinate system, the normal component (red) and current aligned (black) electric field of E_{yGSE} . Also shown is the boundary normal vector in the y_{GSE} - z_{GSE} plane. (Three bottom panels) The x , y and z components of magnetic field in boundary normal coordinate system. Vertical dashed lines ($L_1 - L_4$) mark the zero crossings of the magnetic field components.

system. Since the simulations are in boundary normal coordinate system, the profile of the electric field in Fig. 4 is obtained by transforming it from boundary normal to the GSE system. The boundary normal vector $\hat{n} = -0.05\hat{x}_{GSE} + 0.80\hat{y}_{GSE} - 0.59\hat{z}_{GSE}$ of the highly tilted current sheet in Cluster observations is almost in the y_{GSE} - z_{GSE} plane and shown in the top panel of Fig. 4. Assuming the simulation current sheet to have the same orientation with respect to the GSE coordinate system, the y -component of the electric field in the latter can be obtained from $E_{yGSE} = E_y \sin(\alpha) - E_z \cos(\alpha)$, where α is the angle between

the normal vector and the \hat{y}_{GSE} , with $\cos(\alpha) = 0.8$.

The electric and magnetic field profiles in the Cluster observation (Fig. 1) and EMHD simulation (Fig. 4) are remarkably similar not only in magnitude but also in the scale and pattern of variation. The current sheet crossing, represented by the change in B_x from ≈ -10 nT to ≈ 10 nT in observations (during $\sim 46 : 48 - 46 : 51$, Fig. 1) and simulations (Fig. 4), provides more details of the reconnection in the magnetotail. The half thickness of the current sheet in simulations $\approx 7d_e$ compares well with the observed values $\sim 3 - 5d_e$. The step-like structures of B_x inside the current sheet are present both in simulations and observations, and indicate a filamentary structure in the current sheet.

Associated with the current sheet crossing, E_{yGSE} and Hall field B_y have bipolar forms changing their signs from negative to positive. The positive and negative peaks of the bipolar structures of E_{yGSE} and B_y in observations and simulations are very similar. Consistent with the observations, Fig. 4 shows that E_{yGSE} , given by $E_y \sin(\alpha) - E_z \cos(\alpha)$, is dominated by the normal component of the electric field, $E_z \cos(\alpha)$, due to the tilt of the current sheet with respect to the GSE coordinate system. Line L_4 in Fig. 1 and Fig. 4 show that E_{yGSE} crosses zero earlier than both B_x and B_y , which cross zero simultaneously. The normal component of magnetic field B_z remains positive during the current sheet crossing but is negative just before the current sheet crossing (between L_1 and L_3). The zero crossing of B_z at L_3 coincides with the edge of the current sheet and negative peaks of E_{yGSE} and B_y . Both B_z and B_y have positive values before their first zero crossings at L_1 and L_2 , respectively. In the simulations, the positive B_y on the left of L_2 is due to the crossing of a positive pole (marked by '+' on positive x -side in Fig. 3b) of the new (outer) quadrupole structure of B_y . The positive B_y on the left of L_2 in Fig. 1 can be identified with the new quadrupole and the Cluster observation is consistent with a nested quadrupole structure of the out-of-plane magnetic field.

The formation of the nested structure of quadrupoles of the Hall magnetic field requires not only the presence of multiple sites but also the dominance of one site over the neighboring sites. Simulations with three reconnection sites of equal strength (excited by initializing the simulations with a single wavelength perturbation with three wavelengths fitting in the length of the simulation box along x) show that the out-of-plane magnetic field does not develop nested structure of quadrupoles. Although quadrupole structure of B_y forms at each reconnection site, the inflow to one site and outflow from the neighboring site do not interact

in the manner that results into the nested quadrupole structure. In natural situations, e.g., in the magneto-tail, reconnection at multiple sites is expected, with the one initiated first being dominant over the adjacent sites. Further, in the magnetotail the monotonic decrease of the magnetic field away from Earth (along x) will introduce asymmetry among the multiple reconnection sites, thus leading to the nested Hall field.

In the Cluster observations, the total time of crossing ≈ 6 sec., close to the ion cyclotron period and thus captured the electron dominated physics of reconnection. Since these electron scale observations are by a single spacecraft when the other three spacecrafts were separated by distances much larger than typical electron scales (~ 20 km), the spatial and time variations are not uniquely distinguished. However, the EMHD simulations show that the electron scale structures form very quickly, in a time of the order of tens of electron cyclotron periods, but evolve very slowly after their formation [9]. Thus the structures observed by Cluster are consistent with spatial variations as described above. The forthcoming multi-spacecraft NASA/MMS mission, designed to resolve the electron scales in the magnetosphere and to distinguish between spatial and time variations, will provide key details of the spatio-temporal structure.

The nested quadrupole structure of Hall magnetic field identified in Cluster observations and the underlying mechanism revealed by EMHD simulations focus only on electron scale processes. Many details of the electron scale physics and the connection to the larger scale ion processes remain unexplored. Such studies will require new studies of electron scale physics in simulations, experiments and satellite observations of magnetic reconnection. In particular, the results presented in this Letter provide a critical step for a deeper understanding of reconnection at electron scales using new kinetic simulations that resolve the electron scales clearly and the data for electron scale physics from the upcoming NASA/MMS mission.

-
- [1] B. U. O. Sonnerup, in *Solar System Plasma Physics, vol. 3* (North-Holland, Amsterdam, 1979) pp. 47–108
 - [2] M. E. Mandt, R. E. Denton, and J. F. Drake, *Geophys. Res. Lett.* **21**, 73 (1994)
 - [3] J. R. Wygant, C. A. Cattell, R. Lysak, Y. Song, J. Dombek, J. McFadden, F. S. Mozer, C. W. Carlson, G. Parks, E. A. Lucek, A. Balogh, M. Andre, H. Reme, M. Hesse, and C. Mouikis,

- J. Geophys. Res. **110**, A09206 (2005)
- [4] A. L. Borg, M. Oieroset, T. D. Phan, F. S. Mozer, A. Pedersen, and C. Mouikis, Geophys. Res. Lett. **12**, L19105 (2005)
- [5] Y. Asano, T. Mukai, M. Hoshino, Y. Saito, H. Hayakawa, and T. Nagai, J. Geophys. Res. **109**, A02212 (2004)
- [6] Y. Ren, M. Yamada, S. Gerhardt, H. Ji, R. Kulsrud, and A. Kuritsyn, Phys. Rev. Lett. **95**, 055003 (2005)
- [7] M. Hesse, J. Birn, and M. Kuznetsova, J. Geophys. Res. **106**, 3721 (2001)
- [8] W. Daughton, J. Scudder, and H. Karimabadi, Phys. Plasmas **13**, 072101 (2006)
- [9] N. Jain and A. S. Sharma, Phys. Plasmas **16**, 050704 (2009)
- [10] N. Attico, F. Califano, and F. Pegoraro, Phys. Plasmas **7**, 2381 (2000)
- [11] L. R. O. Storey, Phil. Trans. Roy. Soc. Ser. A **246**, 113 (1953)
- [12] N. Singh, Phys. Rev. Lett. **107**, 245003 (2011)
- [13] N. Singh, J. Geophys. Res. **112**, A07209 (2007)